Supporting information

Ketimine and *β*-ketoenamine Contained Porous Organic Polymer for Adsorbing CO_2 and Catalyzing Knoevenagel Reaction

Guoxin Cui, Yan Li, Guan Yun, Yongzheng Zhao, Peng Gu, Jing Li, Jinghan Zhang, Shuxin Cui, Minghao Liu, Weiqi Zeng, Zhenlu Wang, Jian Jiang

Contents

Section		Page No.
S-1	Experimental methods	S2
S-2	Study of Conformations of BL with Materials Studio	S6
S-3	Characterization of BL	S7
S-4	PXRD of BL-TP-POP	S9
S-6	Morphology studies	S11
S-5	Calculation of surface area with multi-point BET plot	S10
S-7	Linear fitting of the low-pressure Henry region	S12
S-8	Nonlinear Curve fitting with Toth equation	S14
S-9	Studies of Fluorescence	S15
S-10	UV-Vis DRS spectrum of BL-TP-POP and monomers	S16
S-11	Chemical stability studies	S17
S-12	Recyclability of the the adsorbent	S18
S-13	Knoevenagel reaction related graphs	S19
S-14	Reaction condition studies	S20
S-15	CO_2 uptake capacity compared with other materials	S22
S-16	Studies of binding sites with Materials Studio	S23
S-17	References	S24

Section S-1: Experimental methods

Cyclic voltammetry measurement: Cyclic voltammetry (CV) experiment was measured on a CHI 900C in a three-electrode electrochemical cell with a scan rate of 0.10 V s^{-1}. The experiment was conducted in anhydrous acetonitrile with tetrabutylammonium hexafluorophosphate (0.1 M) as supporting electrolyte. The auxiliary electrode was a platinum wire. The reference electrode was based on the AgCl/Ag couple. The working electrode was a glass carbon electrode. Ferrocene/ferrocenium (Fc/Fc^+) redox potential was measured at the end of the experiment to calibrate the pseudo reference electrode as recommended by IUPAC. To prepare the sample for CV measurement, POP powder was dispersed in ethanol with a few droplets of 5 wt% Nafion and stirred for 3h. The suspension was then dropped on the glassy carbon electrode and dried in air to form thin film for measurements.

HOMO and LUMO level are determined as follows[1]:

$$E_{HOMO} = -[E_{ox\_onset} - E(Fc/Fc^+) + 4.8]\ eV$$

$$E_{LUMO} = -[E_{red\_onset} - E(Fc/Fc^+) + 4.8]\ eV$$

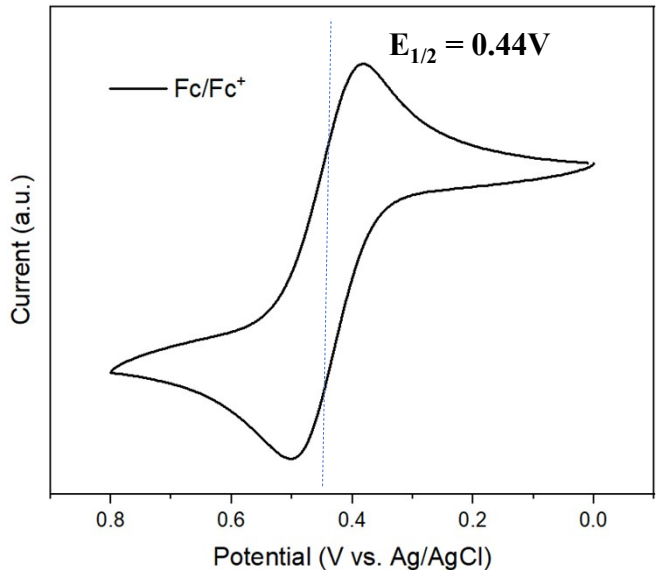

Figure S1. Cyclic voltammetry measurements of ferrocene/ferrocenium couple to calibrate the pseudo reference electrode.

Stability test and recovery methods of POP: The **BL-TP-POP** sample (150 mg) was dispersed in different solvents including water, THF, CH_2Cl_2, aqueous HCl (3 M), aqueous NaOH (3 M). The mixtures were stirred for 24 hours.

The POP samples in water, THF, CH_2Cl_2 were collected by filtration and dried at 120 ℃ under vacuum for 12 hours. The sample in the aqueous HCl solution was washed with water (5 ×10 mL), neutralized with triethylamine/acetone solution (5%, 1×10 mL), washed again with water (5×10 mL), and dried under vacuum at 120°C for 12 h. POP sample in aqueous NaOH solution was washed with water (20×10ml) and dried under vacuum at 120°C for 12 h. These samples were then used for FTIR measurements.

Calculation of isosteric heat of adsorption (Q_{st}): The CO_2 adsorption isotherms measured at 273 K and 298 K were first fitted to the following Toth equation,

$$A = \frac{qbp}{[(1+bp)^t]^{1/t}}$$

Where A is the adsorbed amount in equilibrium (mmol/g); p is the equilibrium pressure of the bulk gas (kPa); q is the saturation capacity of CO_2; b and t are fitting parameters of Toth equation. The isosteric heat of adsorption was calculated from the following equation,

$$Q_{st} = \frac{(lnp_2 - lnp_1)RT_2T_1}{T_2 - T_1}$$

Where R is the gas constant (8.314 J K^{-1} mol^{-1}); T_2 and T_1 are different temperatures; p_2 and p_1 are equilibrium pressures when different amounts of CO_2 (mmol/g) was adsorbed at T_2 and T_1, respectively.

Calculation of selectivity based on Henry's law: The CO_2/N_2 Henry selectivity was calculated from Henry's law under low pressure up to 0.15 bar. The single component of both CO_2 and N_2 adsorption isotherms were fitted linearly. Then, their slope ratio showed the corresponding selectivity of CO_2/N_2.

Calculation of percentage yield of the product of Knoevenagel reaction: A series of benzylidenemalononitrile/benzene solutions with different concentrations were prepared. After running in GC-MS, the working curve was made based on the integral areas of different solutions. The actual yield of product of Knoevenagel reaction in this study was calculate based on the working curve. Then the percentage yield was calculated from the following equation,

$$\text{Yield (\%)} = \text{yield}_{\text{actual}} / \text{yield}_{\text{theoretical}}$$

Determination of average lifetime of fluorescence: The y-axis of fluorescence decay plot was first converted to logarithmic scale and normalized. The decay curve was then fitted with the following EXPDEC2 function,

$$y = A_1 e^{-x/t_1} + A_2 e^{-x/t_2}$$

Where y is the normalized log fluorescence intensity as a function of time x; t_1 and t_2 are fluorescence lifetimes of the 1st and 2nd decay component; A_1 and A_2 are the fractional amplitude of corresponding component. After A_1, t_1, A_2 and t_2 were obtained from the fitting, the average lifetime (t) of the fluorescence was calculated as the following function,

$$t = \frac{A_1 t_1^2 + A_2 t_2^2}{A_1 t_1 + A_2 t_2}$$

Computational Methodology:

Location simulations were performed by using a Sorption module of Materials Studio. The Metropolis Monte Carlo method was chosen for the calculation of binding locations. Universal force field (UFF) was used for the energy calculation, and the charge equilibration (Qeq) method was chosen for the calculation of point atomic charges. Ewald & Group was utilized as the electrostatic interaction method. Simulation temperature: 273 K; equilibrium steps: 100000, production steps: 10000000.

DFT calculation was performed by the DMol^3 program in the Materials Studio. The exchange-correlation interactions were treated according to the generalized gradient approximation (GGA) parameterized by the Becke-Lee-Yang-Parr function (BLYP). A doble numerical basis set with polarization function (DNP) was used in DFT calculation without any symmetry constraints. Van der Waals dispersion corrections were treated by the Grimme DFT-D method. All-electron numerical method was selected for core treatment. A smearing of 0.005 Ha was applied for the structure optimization. SCF tolerance was set as 1.0×10^{-6}.

Conformer calculation was performed by the Conformers module of Materials Studio. Systematic grid scan was used as search method. Universal force field (UFF) was used for energy calculation and charge equilibration (Qeq) method was chosen for the calculation of point atomic charge. Atom based was utilized as the electrostatic interaction method.

Section S-2. Study of Conformations of BL with Materials Studio

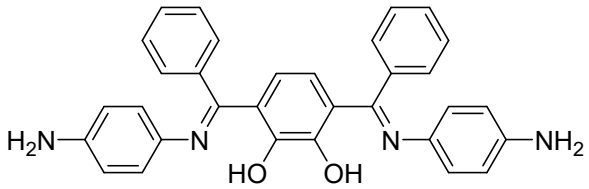

Figure S2. The structure of **BL**

Because of steric-hindrance effect, the ketimine phenyl rings prevented **BL** from giving planar structure. To study the conformation of **BL**, we used Materials Studio software package to construct model of the structure (Hydrogen bonding between -OH and -N= was set in the model, because ^{1}H NMR of **BL** showed the chemical shift of proton on -OH was 15.54 ppm, which indicated intramolecular hydrogen bonding was formed.). Calculation, with Conformers module (universal forcefield), exhibited there were at least 24928 conformers with similar energy, and all these conformers were nonplanar and twisted. The result indicated that **BL** was nonplanar and very flexible although all double bonds were conjugated in the system. Several conformers with calculated energy were shown below:

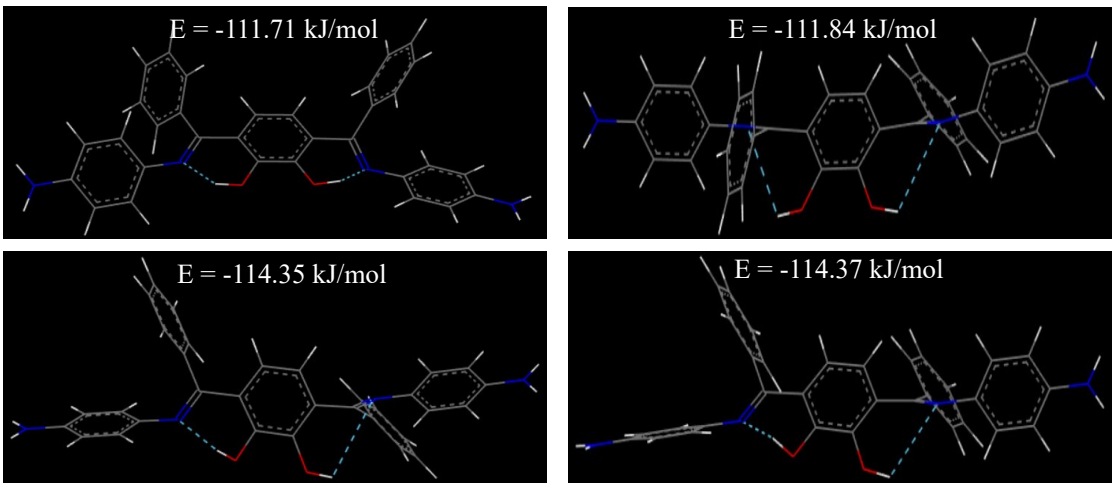

Figure S3. Several conformers of BL with calculated energy

Section S-3. Characterization of BL

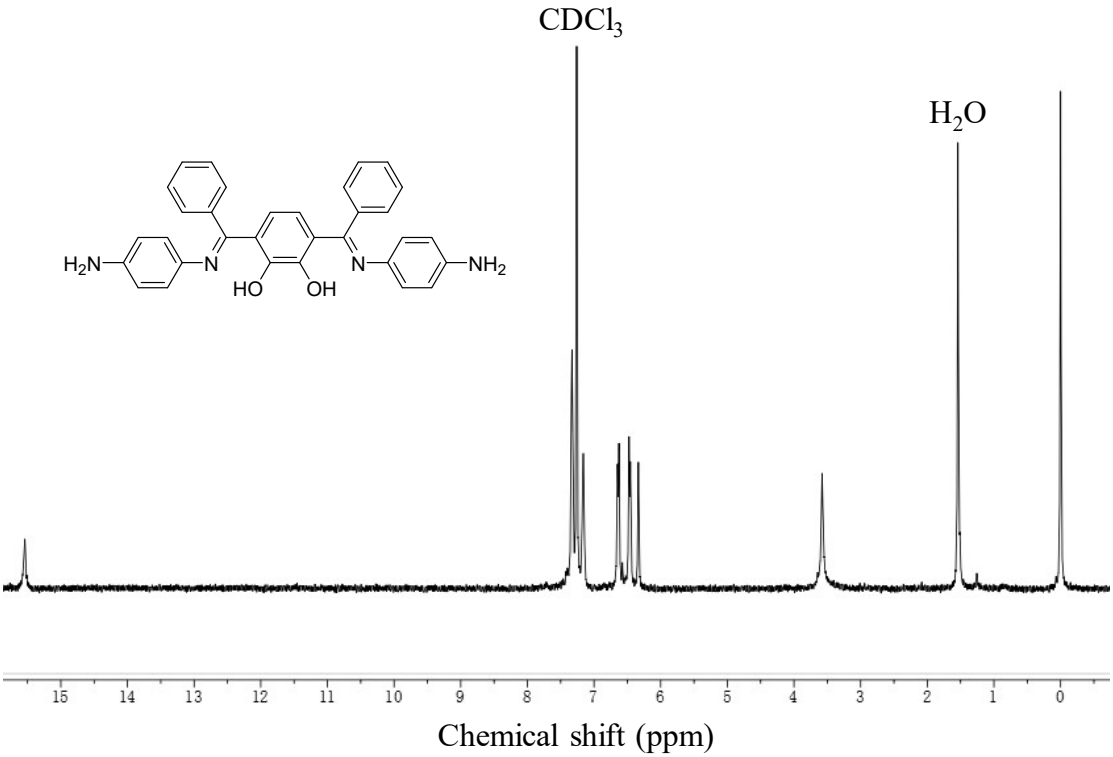

Figure S4. ^{1}H NMR spectrum of **BL** in $CDCl_3$ (400 MHz, 298K).

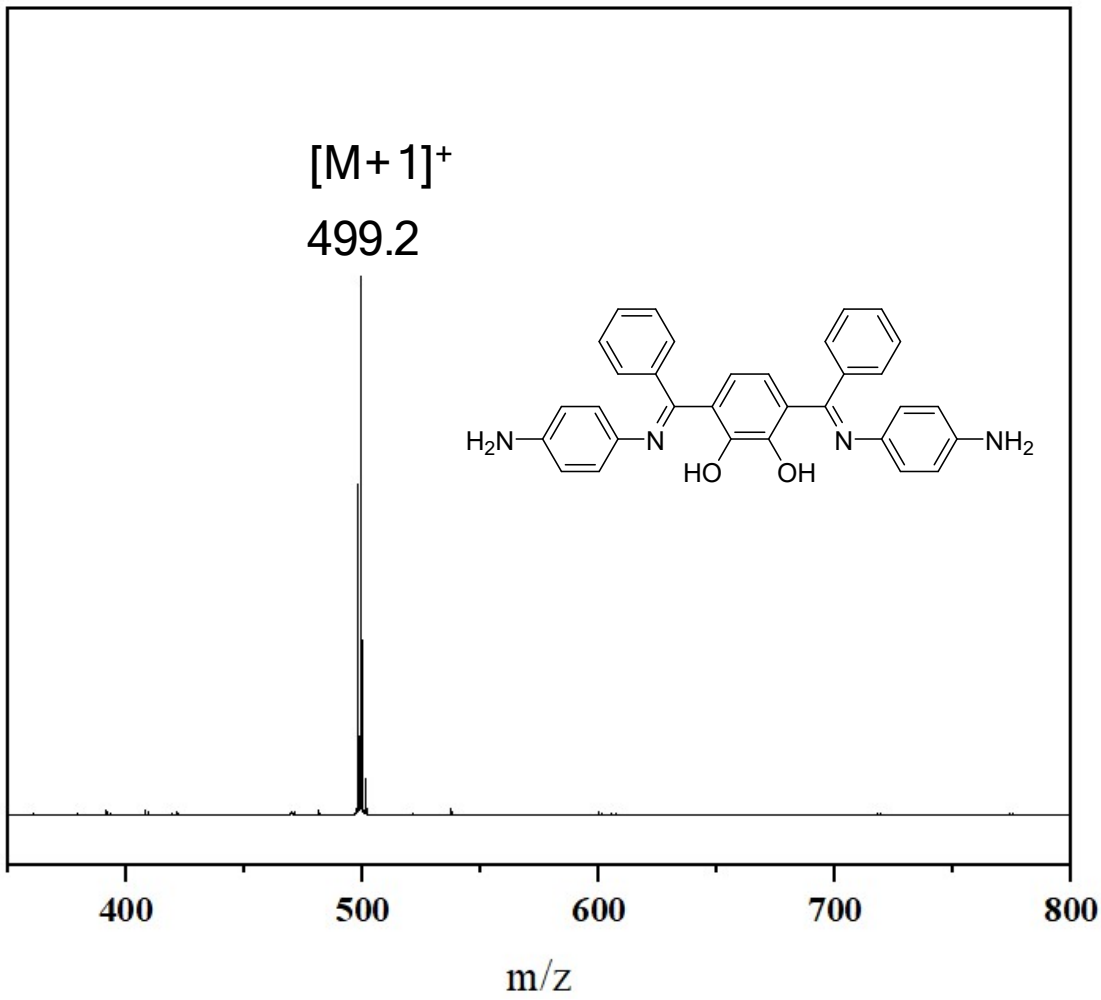

Figure S5. MOLDI-TOF MS spectrum of BL

Section S-4. PXRD of BL-TP-POP

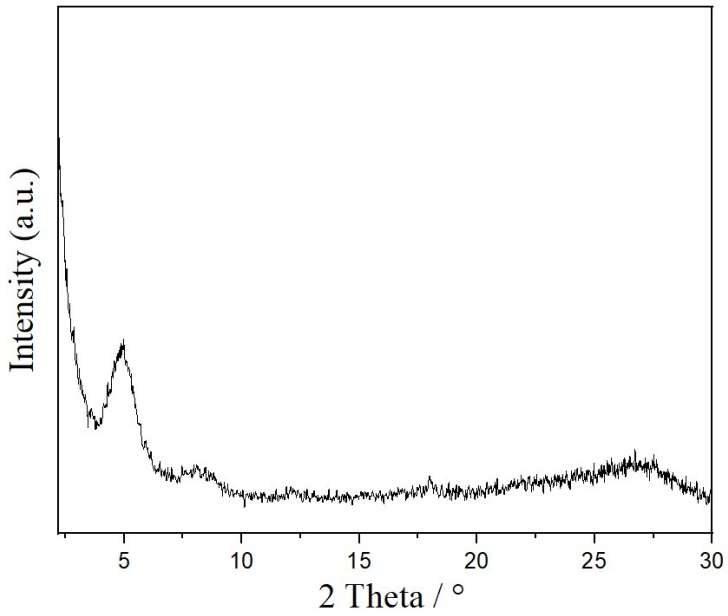

Figure S6. PXRD of **BL-TP-POP**

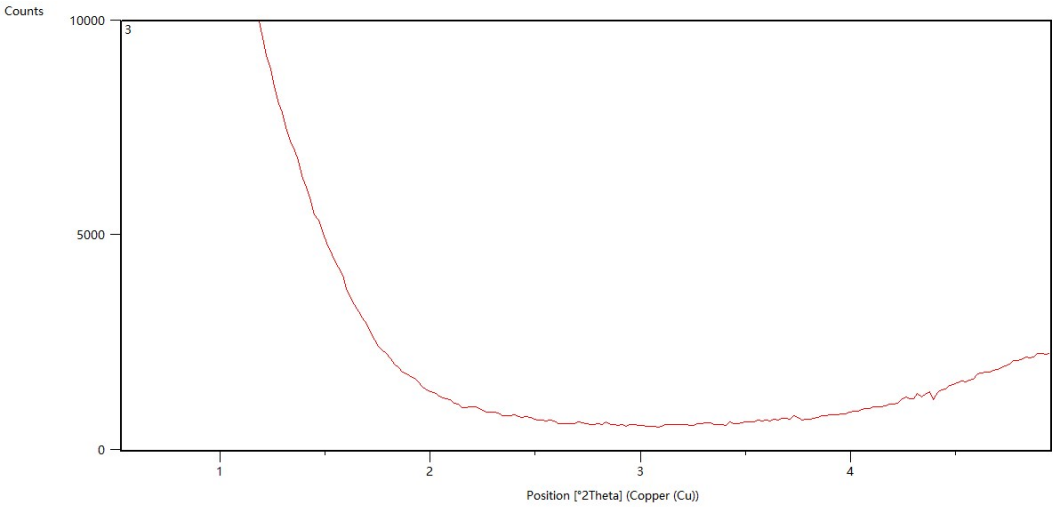

Figure S7. Small angle X-ray Scattering of **BL-TP-POP**

Section S-5. Calculation of surface area with multi-point BET plot

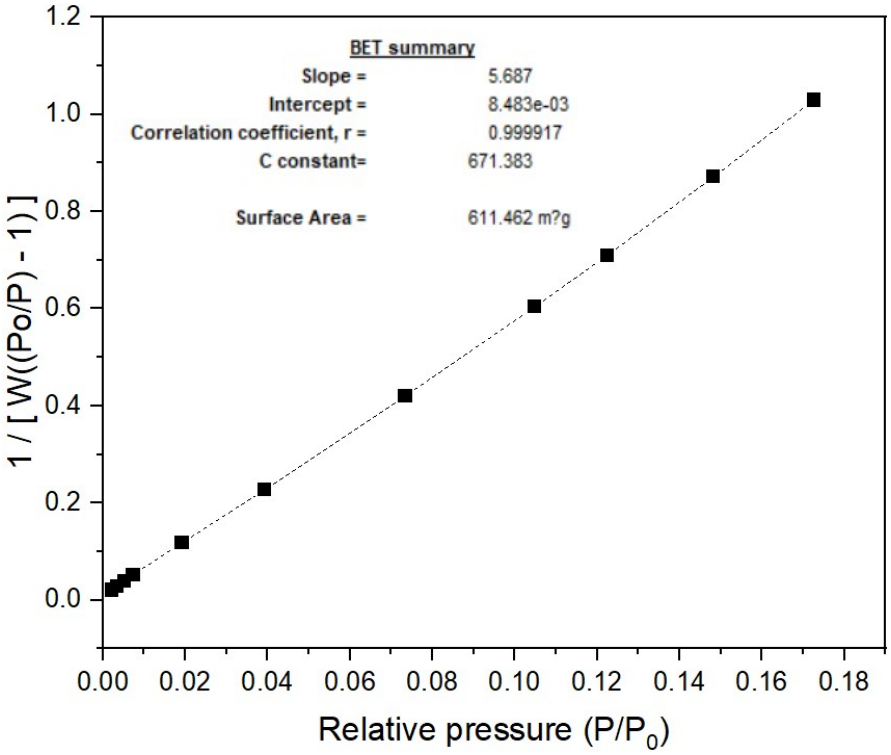

Figure S8. Plot of linear region for the BET equation of **BL-TP-POP**.

Section S-6: Morphology studies

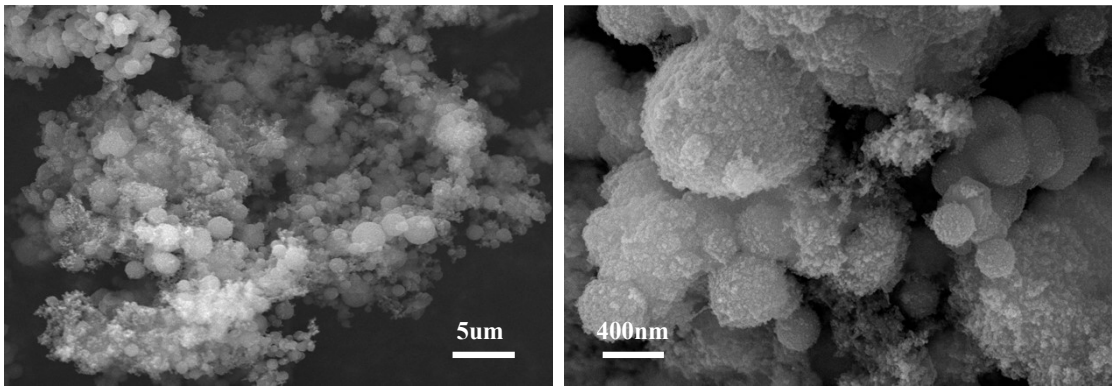

Figure S9. SEM images of **BL-TP-POP**

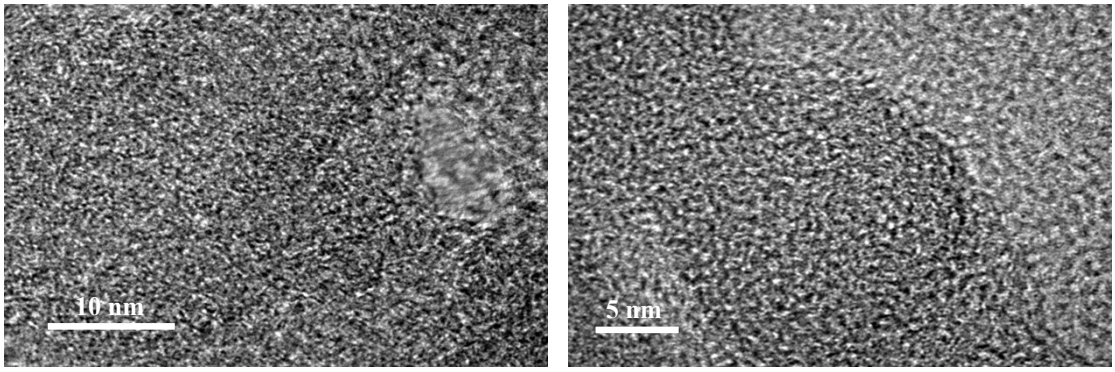

Figure S10. HR-TEM images of **BL-TP-POP**

Section S-7. Linear fitting of the low-pressure Henry region

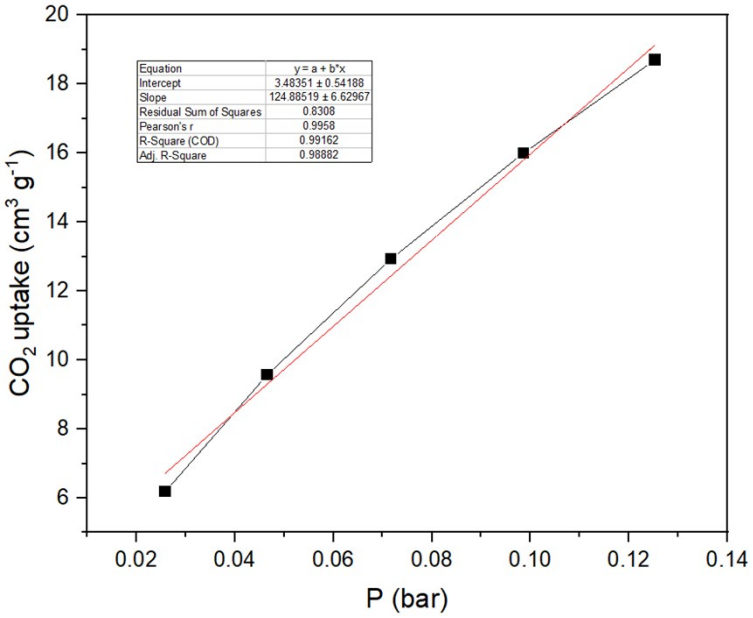

Figure S11. Linear fitting of the low-pressure Henry region of CO_2 adsorption isotherms on **BL-TP-POP** measured at 273 K.

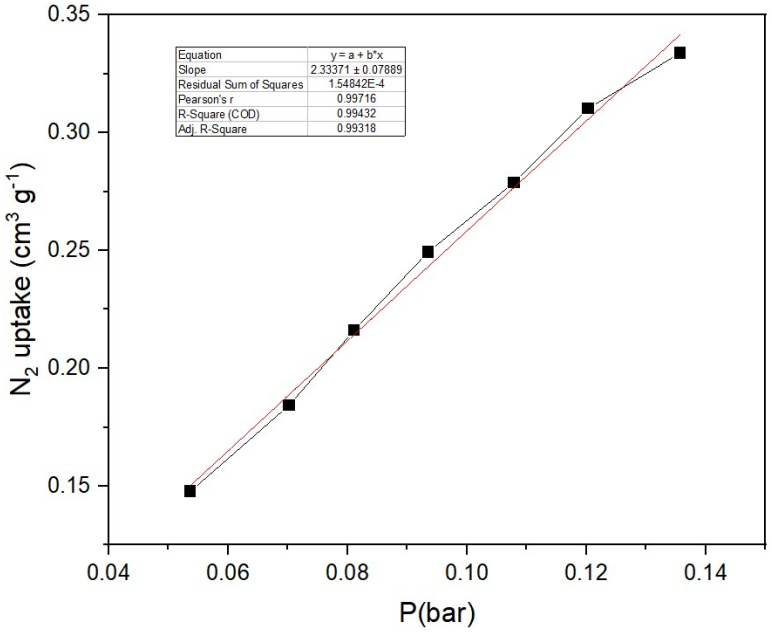

Figure S12. Linear fitting of the low-pressure Henry region of N_2 adsorption isotherms on **BL-TP-POP** measured at 273 K.

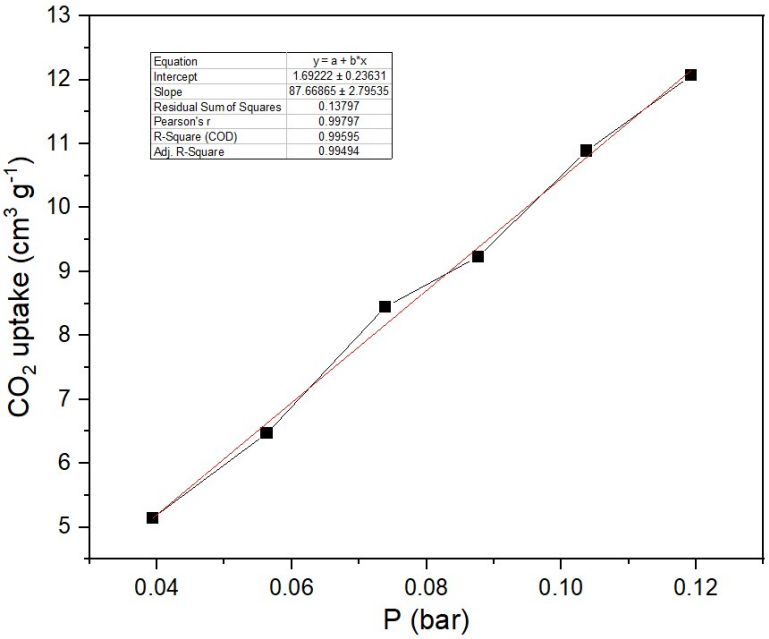

Figure S13. Linear fitting of the low-pressure Henry region of CO_2 adsorption isotherms on **BL-TP-POP** measured at 298 K.

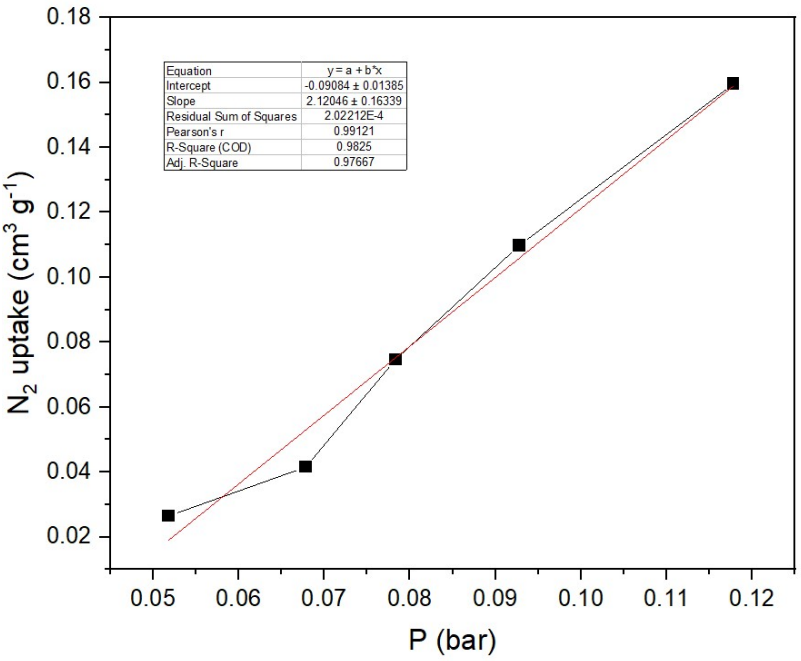

Figure S14. Linear fitting of the low-pressure Henry region of N_2 adsorption isotherms on **BL-TP-POP** measured at 298 K.

Section S-8. Nonlinear Curve fitting with Toth equation

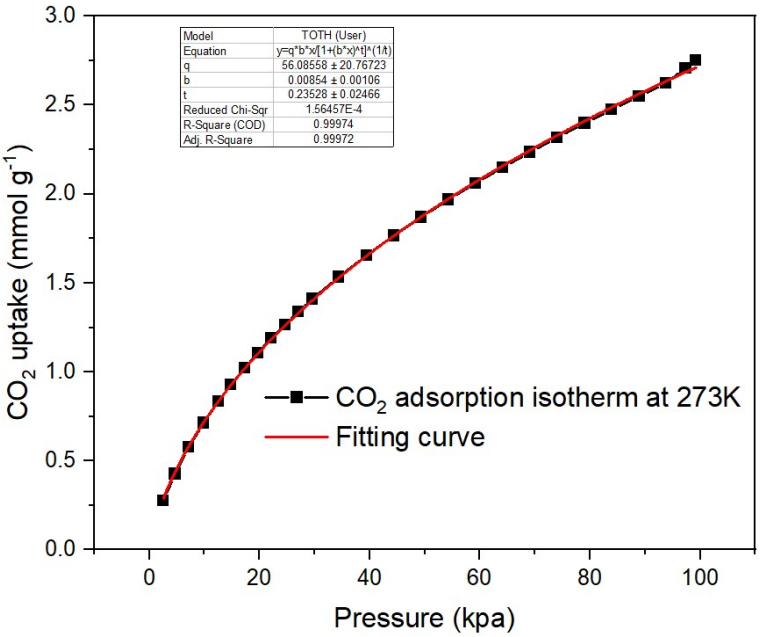

Figure 15. Nonlinear curve fitting of CO_2 adsorption isotherm at 273K with Toth equation.

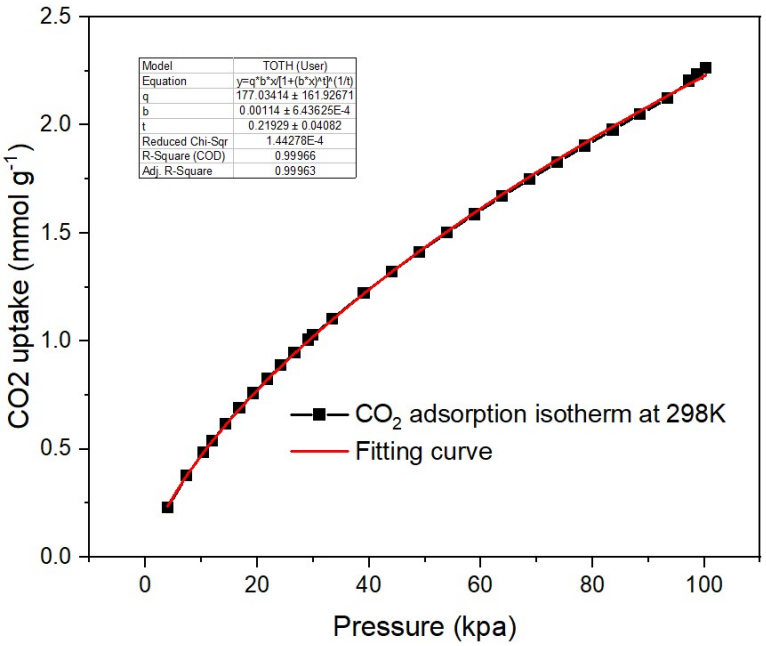

Figure 16. Nonlinear curve fitting of CO_2 adsorption isotherm at 298K with Toth equation.

Section S-9. Studies of Fluorescence

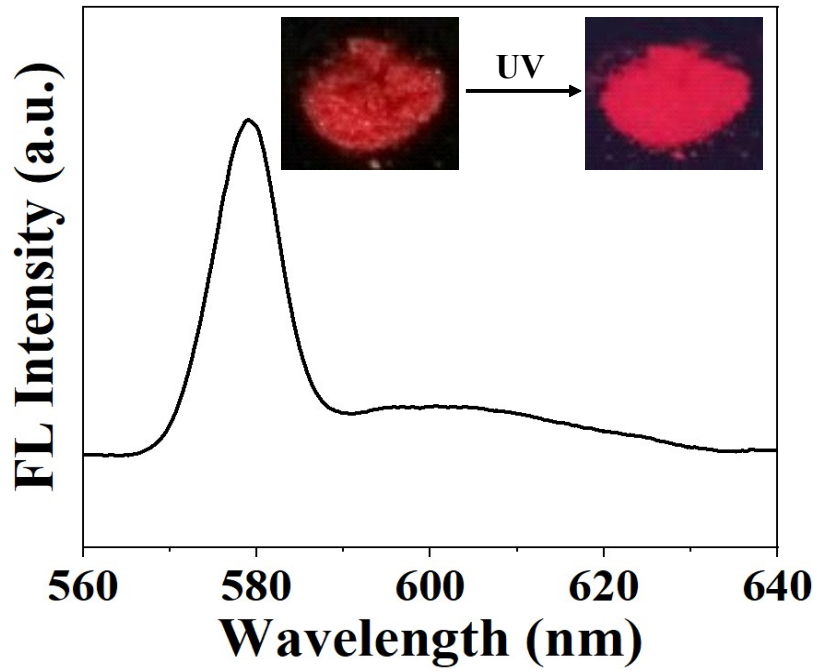

Figure S17. Fluorescence emission spectrum of BL-TP-POP (insert: photographs of POP powder before and after irradiation under 365 nm UV lamp).

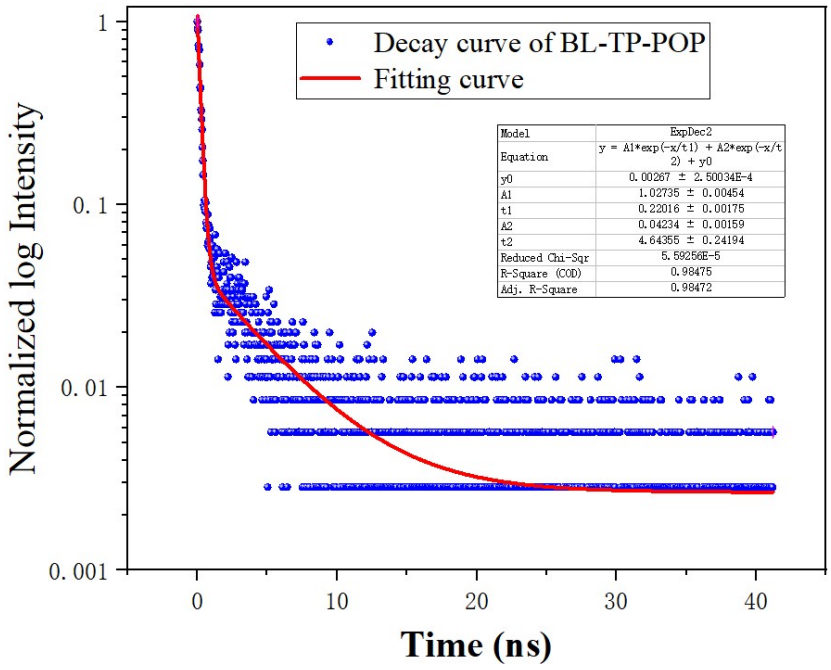

Figure 18. Time-resolved fluorescence lifetime decay spectra and curve fitting with EXPDEC2 function.

Section S-10. UV-Vis DRS spectrum of BL-TP-POP and monomers

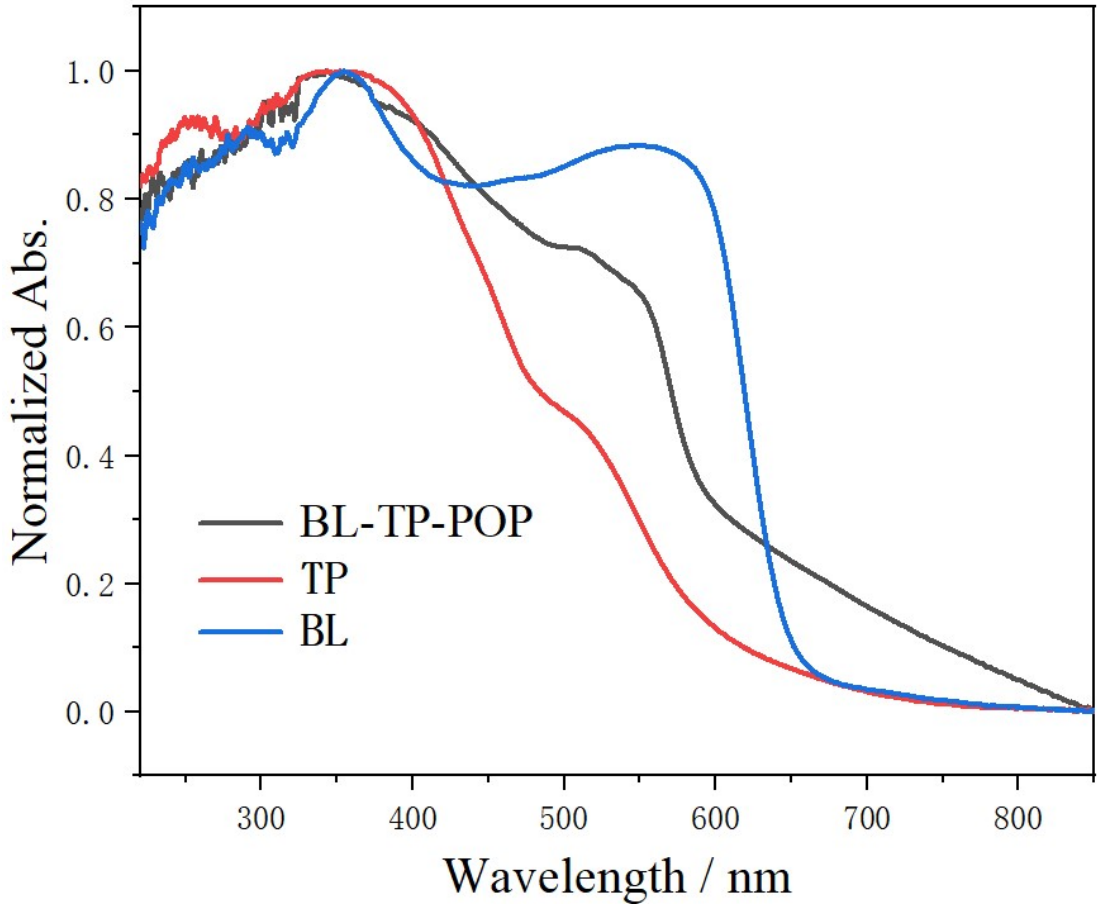

Figure S19. UV-Vis DRS spectra of **BL-TP-POP**, **TP** and **BL**.

Section S-11: Chemical stability studies

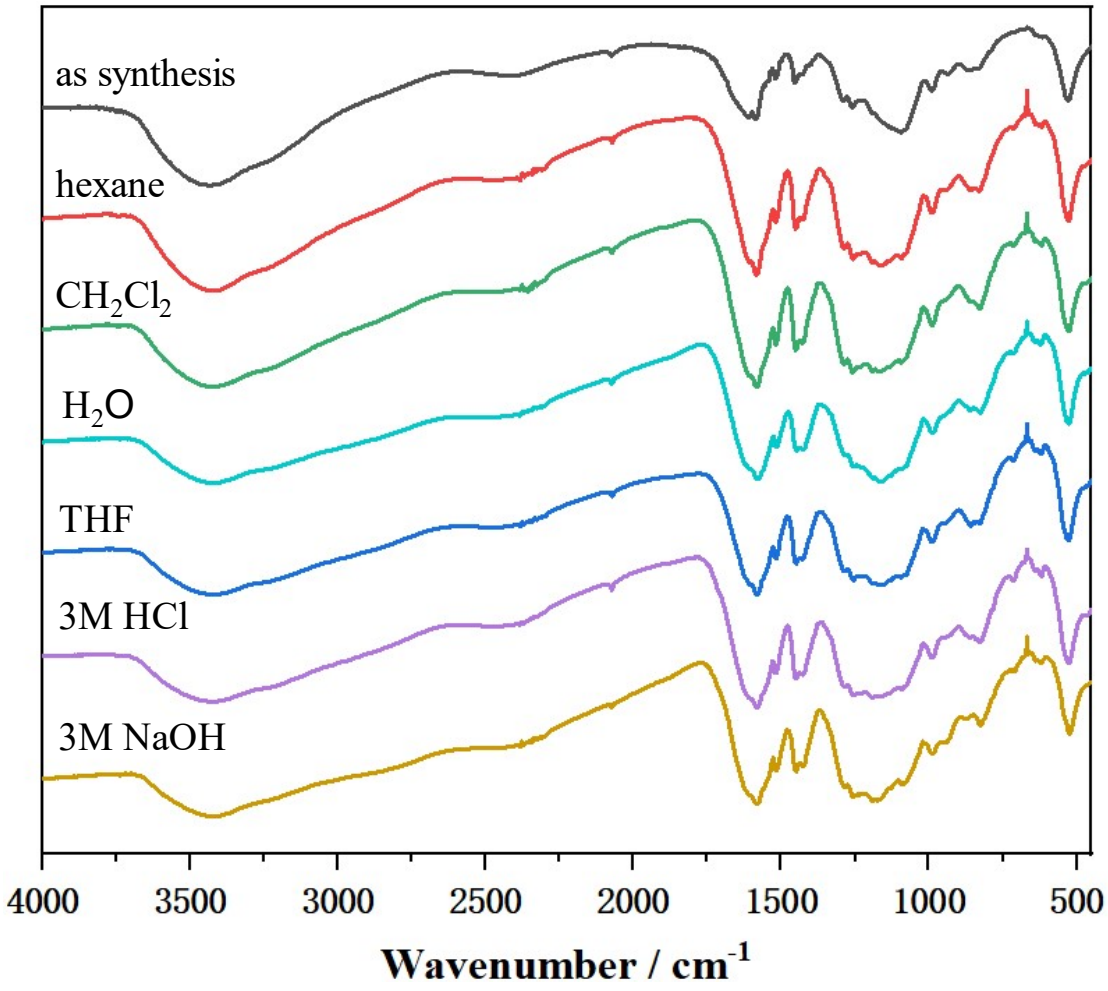

Figure S20. FT-IR spectra of recovered **BL-TP-COF** after immersed in different solvents (7 days for hexane, CH_2Cl_2, H_2O, THF and 3M HCl; 1day for 3M NaOH).

Section S-12. Recyclability of the the adsorbent

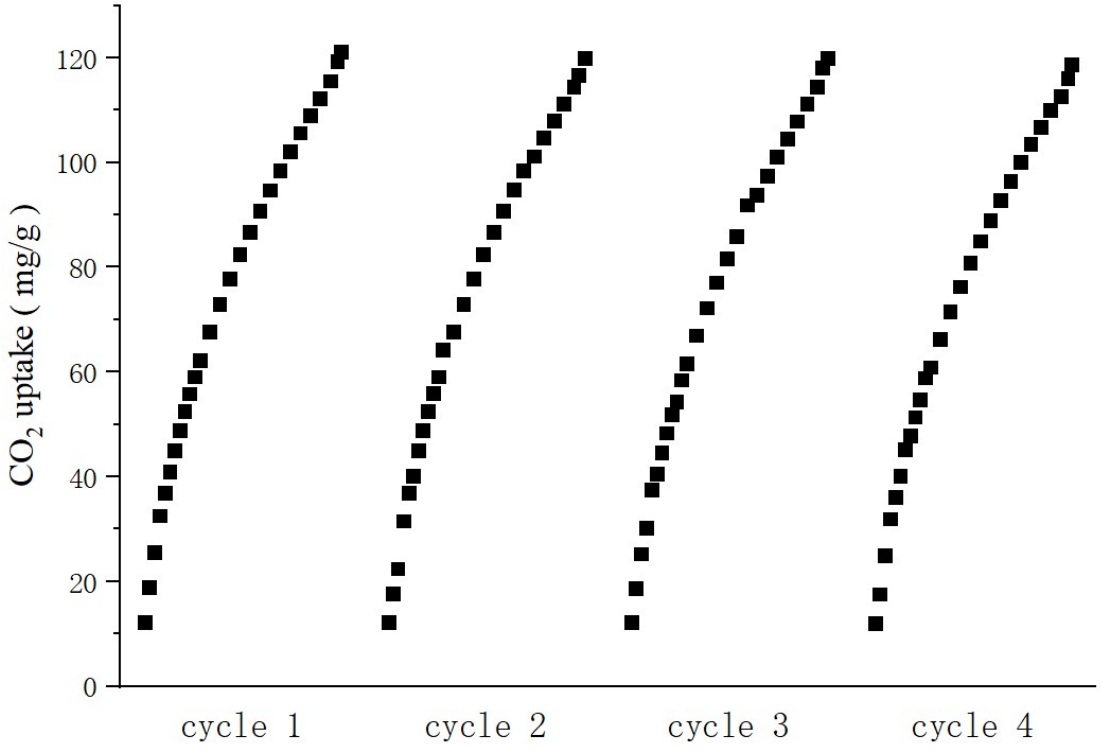

Figure S21. Recycle of CO_2 adsorption by **BL-TP-POP** at 273K.

Section S-13. Knoevenagel reaction related graphs

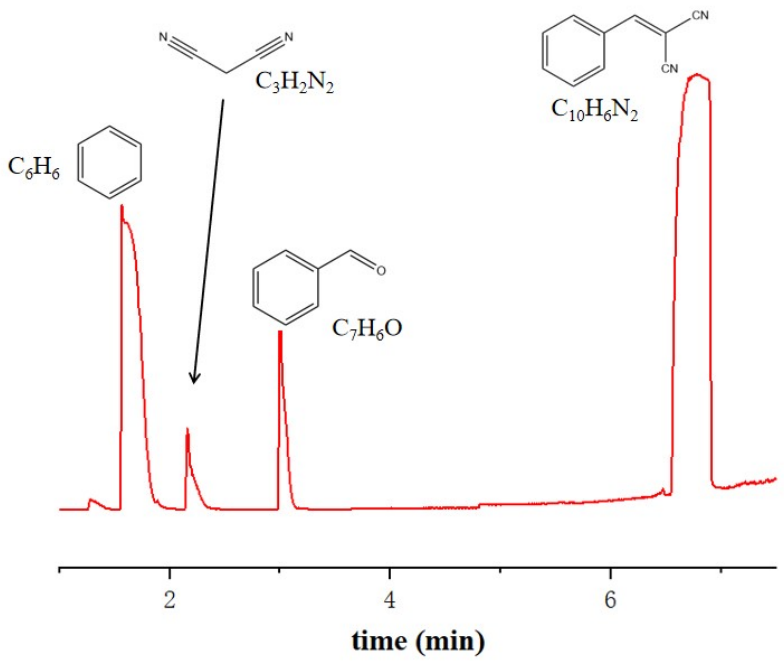

Figure S22. Typical chromatogram map for the product of Knoevenagel reactions.

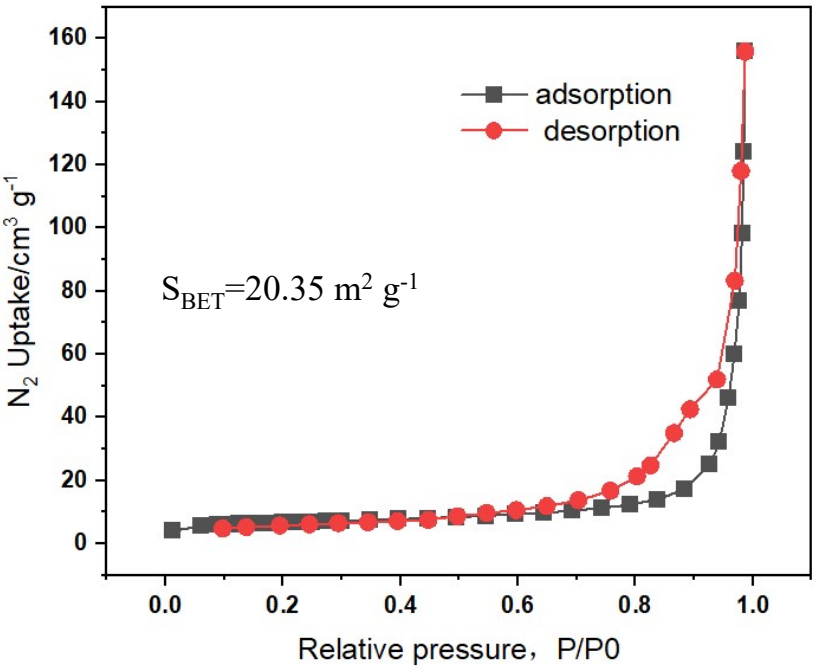

Figure S23. Nitrogen sorption isotherm of **BL** measured at 77K.

Section S-14. Reaction condition studies

Table S1. Synthesis of BL-TP-POP under different reaction conditions.

Entries	Solvents	Catalyst（HOAc）		S_{BET}	Form
		Consentration（M）	Volume（ml）	(m^2 g^{-1})	
1	o-DCB/ n-BuOH (2ml/2ml)	1	0.2	217.2	amorphous
2	o-DCB/ n-BuOH (2ml/2ml)	1	0.4	223.1	amorphous
3	o-DCB/ n-BuOH (2ml/2ml)	1	0.8	321.7	amorphous
4	o-DCB/ n-BuOH (2ml/2ml)	3	0.2	474.8	amorphous
5	o-DCB/ n-BuOH (2ml/2ml)	3	0.4	443.9	amorphous
6	o-DCB/ n-BuOH (2ml/2ml)	3	0.8	611.5	amorphous
7	o-DCB/ n-BuOH (3ml/1ml)	3	0.2	270.9	amorphous
8	o-DCB/ n-BuOH (1ml/3ml)	3	0.4	425.3	amorphous
9	Mesitylene/1,4-dioxane(1ml/3ml)	3	0.8	51.9	amorphous
10	Mesitylene/1,4-dioxane(2ml/2ml)	3	0.8	14.6	amorphous

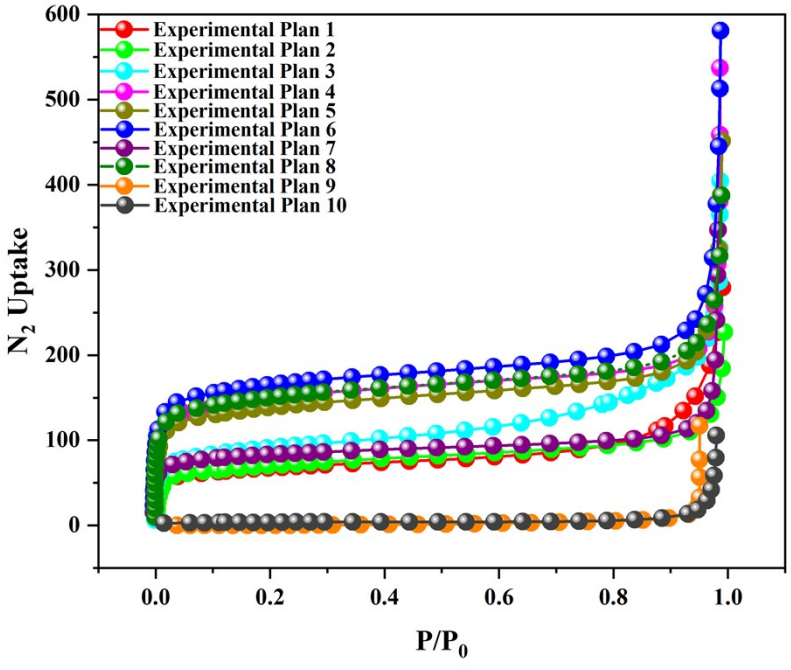

Figure S24. Nitrogen sorption isotherm measurement at 77K of different experimental plans.

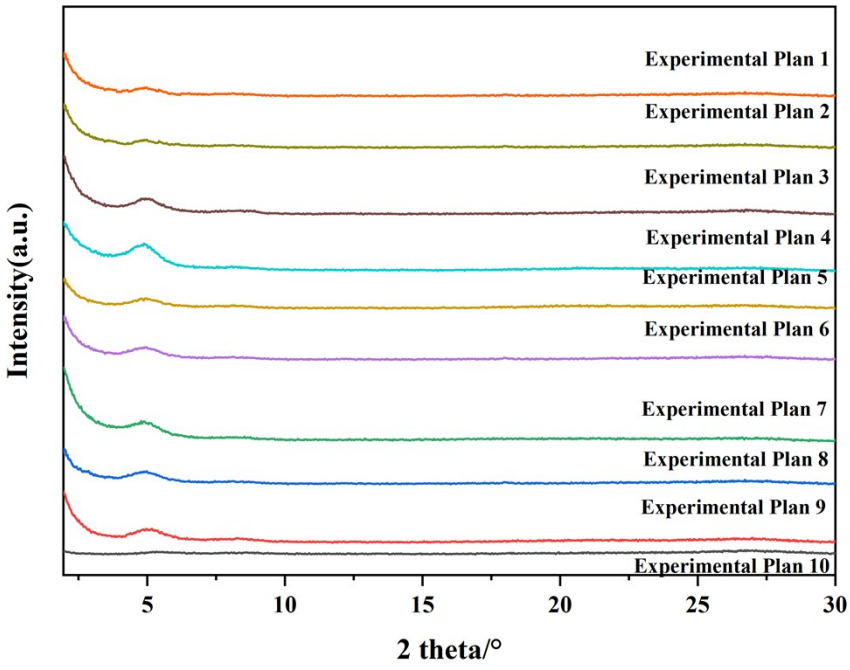

Figure S25. PXRD profiles of different experimental plans.

Section S-15: CO_2 uptake capacity compared with other materials.

Table S2. CO_2 uptake capacities of different adsorbents

Porous Materials	S_{BET} ($m^2\ g^{-1}$)	CO_2 uptake at 273K ($mg\ g^{-1}$)	CO_2 uptake at 298K ($mg\ g^{-1}$)	CO_2/N_2 Selectivity	References
BL-TP-POP	611.46	121.01	99.63	53.53	this paper
NPOF-4	1249	110	61.6	27	[2]
Azo-COP-1	635.8	107.36	65.12	63.7	[3]
PNOP-1	830	176	106.48	52.1	[4]
TMP1	923	154	89.76	64	[5]
TNHCP1	848	127.16	96.8	30	[6]
CMP-1-$(OH)_2$	1043	79.2	47.08	45.2	[7]
NTP	1067	151.8	80.08	18	[8]
NPOP	773	91.96	59.84	30	[9]
azo-COP-2	729	112.2	67.32	109.6	[10]
PECONF-3	851	153.56	108.68	77	[11]

Section S-16: Studies of binding sites with Materials Studio

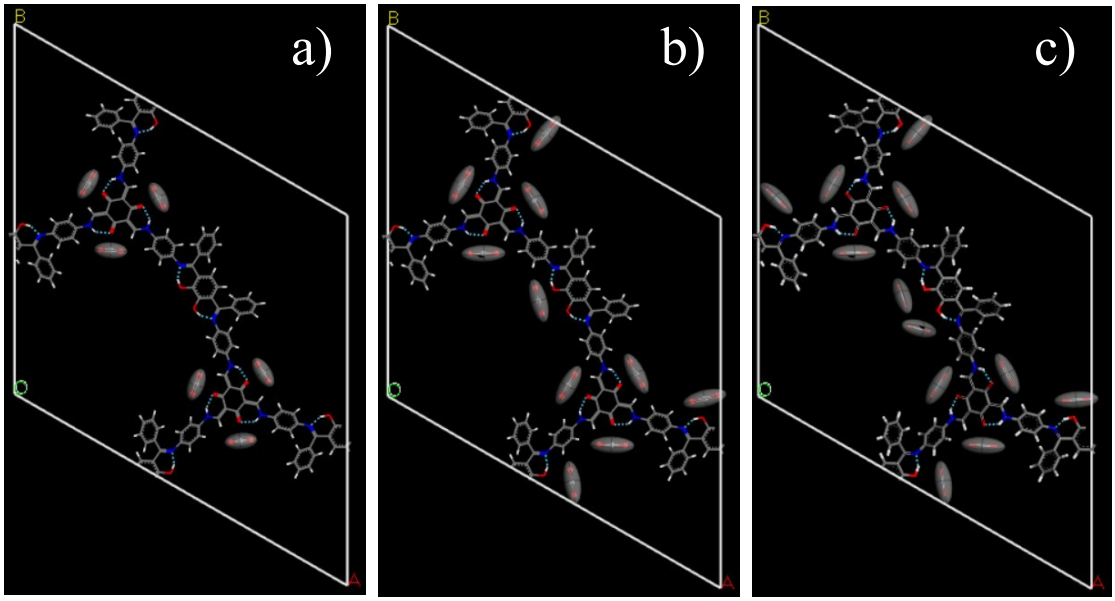

Figure S26. Simulation of binding sites with different numbers of CO_2 molecules in a unit cell. a) Six CO_2 molecules in a unit cell; b) Ten CO_2 molecules in a unit cell; c) Twelve CO_2 molecules in a unit cell.

Section S-17: References

1. R. Chen, J. Shi, Y. Ma, G. Lin, X. Lang and C. Wang, *Angew. Chem. Int. ed.,* 2019, **58**, 6430.
2. T. Islamoğlu, M. G. Rabbani and H. M. El-Kaderi, *J. Mater. Chem. A,* 2013, **1**, 10259.
3. H. A. Patel, S. H. Je, J. Park, Y. Jung, A. Coskun and C. T Yavuz, *Chem. Eur. J*., 2014, **20**, 772.
4. J. Yan, B. Zhang, S. Guo and Z. Wang, *ACS Appl. Nano Mater.,* 2021, **4**, 10565.
5. R. Bera, S. Mondal and N. Das, *Micropor. Mesopor. Mat.,* 2018, **257**, 253.
6. A. Hassan, S. Goswami, A. Alam, R. Bera and N. Das, *Sep. Purif. Technol.,* 2021, **257**, 117923.
7. R. Dawson, D. J. Adams and A. I. Cooper, *Chem. Sci.,* 2011, **2**, 1173.
8. H. Ma, J. J. Chen, L. Tan, J.-H. Bu, Y. Zhu, B. Tan and C. Zhang, *ACS Macro Lett.,* 2016, **5**, 1039.
9. A. Giri, N. N. Patil and A. Patra, *Chem. Commun.,* 2021, **57**, 4404.
10. H. A. Patel, S. H. Je, J. Park, D. P. Chen, Y. Jung and C. T. Yavuz, *Nat. Commun.,* 2013, **4**, 1357.
11. P. Mohanty, L. D. Kull and K. Landskron. *Nat. Commun.*, 2011, **2**, 401.